JOC The Journal of Organic Chemistry

Article

pubs.acs.org/joc

The Influence of the π-Conjugated Spacer on Photophysical Properties of Difluoroboranyls Derived from Amides Carrying a Donor Group

Anna Maria Grabarz,[†] Adèle D. Laurent,[‡] Beata Jędrzejewska,[§] Anna Zakrzewska,[§] Denis Jacquemin,[*,‡] and Borys Ośmiałowski[*,§]

[†]Faculty of Chemistry, Wrocław University of Technology, Wyb. Wyspiańskiego 27, PL-50370 Wrocław, Poland

[‡]Laboratoire CEISAM, UMR CNRS 6230, Université de Nantes, 2 Rue de la Houssinière, BP92208, 44322 Cedex 3 Nantes, France

[§]Faculty of Chemical Technology and Engineering, UTP University of Science and Technology, Seminaryjna 3, PL-85326 Bydgoszcz, Poland

Supporting Information

ABSTRACT: A series of difluoroboranyls derived from amides carrying a variable π-conjugated spacer between the electron-donating (D) and electron-accepting (A) groups was synthesized and characterized with ^{1}H, ^{11}B, ^{13}C, ^{15}N, and ^{19}F NMR, electronic absorption, fluorescence spectroscopies, and first-principle calculations. The D-to-A distance in the series varied from 1.5 to 4.5 Å, causing bathochromic shifts of both the absorption and fluorescence maxima by more than 120 and 213 nm, respectively. These trends are rationalized by quantum-mechanical calculations that allow for quantification of the charge-transfer distance. Theoretical calculations were also performed to determine the vibronic couplings and thus to reproduce the experimental band shapes.

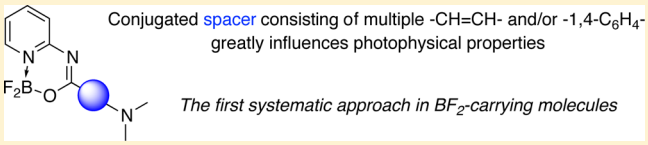

INTRODUCTION

BODIPY dyes are fluorophores presenting sharp absorption and emission bands, high fluorescence quantum yields, and valuable photostabilities. Consequently, their development and their use as molecular probes have been in the limelight over the past decade. The potential of BF_2 dyes was demonstrated in several fields of science as, for example, photodynamic therapy,[1] microscopy,[2,3] molecular probing,[4] drug delivery,[5] laser dyes,[6,7] and more. For designing difluoroboranyls or, more generally, other photoactive compounds, their properties should first be known and understood, a task for which model structures are undoubtedly useful. Several groups of relatively simple BF_2-carrying models have been developed: boron diketonates,[8−10] boron diiminates,[11−13] unsymetric ketoiminates,[14−16] as well as formazanes[17] and boranils.[18−20] In addition, the optical properties of fluorescent compounds may be tuned by different techniques, e.g., the addition of side substituents,[16] benzoannulation,[15,21] extension of the π-conjugated pathway, stiffening of the lateral rings, and the replacement of the atoms that bind Lewis acid in these fluorophores. For the BODIPY dyes, modification at the boron group is also possible.[22]

With the aim of significantly tuning the absorption and emission wavelengths, the structural functionalization at opposite sides of the molecule is especially useful for obtaining compounds exhibiting intramolecular charge transfer (ICT). This is typically achieved by applying electron donor (D) and electron acceptor (A) groups on opposite ends of the molecular π-conjugated skeleton. Of course, the strength of both D and A groups as well as the nature of the π-conjugated spacer separating these groups are important parameters controlling the photophysical properties. The most common spacers are *p*-phenylene and *p*-phenylenevinylene (styryl), which were intensively used in BODIPY dyes.[23−31] The 4,4′-diphenyl spacer is also used in D−A molecules, though less frequently,[32] whereas other π-conjugated spacers (fluorenyl or other aromatics) remain much less explored. If BODIPY dyes in which the donating group is directly attached to the pyrrole rings are known[33] and have been tested for cation binding in both solution[34,35] and living cells,[36] no systematic study of the influence of variable spacer on the photophysical properties of BF_2-carrying molecules has appeared to date. The present contribution aims to fill this gap. Besides the intensively investigated BODIPY dyes, there are several other fluorescent compounds carrying a BF_2-group.[15,16,18,20,37,38] As they remain much less investigated to date, we focused here on molecules that are amide-based difluoroboranyls (see Scheme 1). Until now, no more than 15 molecules of this family have been synthesized[37−40] so we can safely state that further explorations are welcome. In the current study, we have used pyridine as the common heterocycle that is able to interact with the BF_2 moiety by its lone electron pair stabilizing a six-membered ring with an $NB(F_2)O$ pattern that appeared in several previous investigations.[18,41−53]

Compounds exhibiting ICT[54−57] are sensitive to both environment and structural changes and are still being sought

Received: November 24, 2015
Published: February 19, 2016

 © 2016 American Chemical Society

DOI: 10.1021/acs.joc.5b02691
J. Org. Chem. 2016, 81, 2280−2292

Scheme 1. Studied Compounds B1−B7

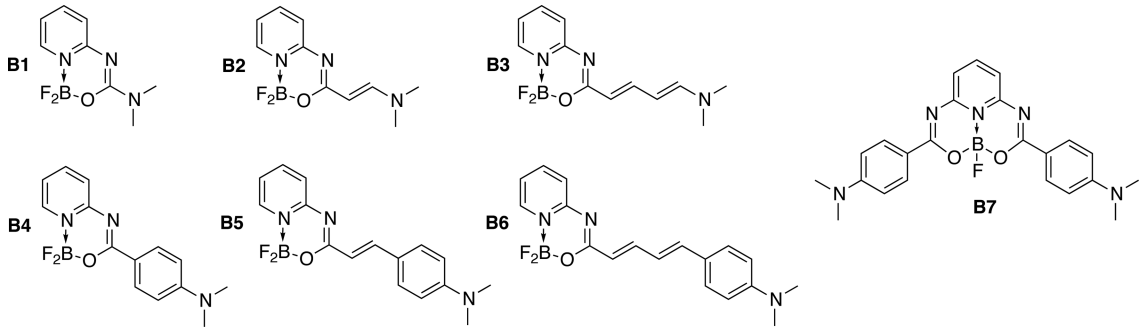

Table 1. Main Photophysical Parameters[a] for Compounds B1−B7

no.	λ_{max}^{Ab}	ε	λ_{max}^{Fl}	$\Delta\nu$	Φ_{Fl}	τ_1, α_1	τ_2, α_2	χ^2	${}^1k_r$	${}^2k_r$	${}^1k_{nr}$	${}^2k_{nr}$
B1	266.5, 334.5	22100, 13500	382	3717	0.648	0.199, 1.14	4.932, 98.86	1.46	17.93	0.59	3.23	0.14
B2	311.0, 389.5	15700, 50100	421	1921	0.325	0.433, 16.96	1.296, 83.04	1.11	4.11	1.09	1.90	0.66
B3	336.5, 454.5	7950, 56200	492	1677	0.038	0.037, 46.45	0.233, 53.55	1.35	5.68	0.70	26.46	4.22
B4	292.5, 404.0	8700, 51000	459	2966	0.685	0.714, 9.49	2.331, 90.51	1.35	5.83	1.05	0.82	0.32
B5	309.5, 441.5	11100, 45800	527	3675	0.186	0.327, 13.95	1.125, 86.05	1.11	2.99	0.77	2.76	0.81
B6	328.5, 460.5	14300, 48000	595	4909	0.098	0.055, 12.91	0.728, 87.09	1.46	10.10	0.59	17.17	1.32
B7	366.0, 451.5	39500, 47800	484	1487	0.385	0.193, 6.14	1.899, 93.86	1.19	6.87	1.30	4.49	0.39

[a]Absorption (λ_{max}^{Ab}; nm), maximum extinction coefficient (ε; 10^4 M^{-1} cm^{-1}), fluorescence maxima (λ_{max}^{Fl}, nm), Stokes shift ($\Delta\nu$, cm^{-1}), fluorescence quantum yield (Φ_{Fl}), fluorescence lifetime (τ; ns), its amplitude (α), and correlation coefficient (χ^2), radiative (k_r, 10^8 s^{-1}), and nonradiative (k_{nr}; 10^9 s^{-1}) rate constants for the compounds under study.

after. These compounds usually present a push−pull structure. In particular, the distance between the acceptor and donor group is a crucial parameter as it drives molecular properties of such compounds.[58] As stated above, various spacers in difluoroboranyl D−A structures have already been described.[28,59] However, to date, the number of spacers between the electron-donating substituent and the fluorogenic center is limited, and to the best of our knowledge, no previous work systematically tackled structures similar to those represented in Scheme 1. Here, we use both experiment and theory to investigate the impact of using a variable molecular length of π-conjugation path that includes double CC bonds and a *p*-phenylene moiety. In addition, a D−A−D difluoroboranyl, **B7**, was designed to ascertain how the presence of two strong electron-donating groups influence the photophysical properties of these molecules compared to dipolar D−A structures.

■ RESULTS AND DISCUSSION

Photophysical Properties. The structures of the studied compounds **B1**−**B7** are shown in Scheme 1, and the detailed synthetic routes of amides (**A1**−**A7**), precursors of difluoroboranyls, and **B1**−**B7** are described in the Experimental Section. Table 1 collects the photophysical data for investigated compounds, and Figures 1 and 2 show the electronic absorption and normalized fluorescence spectra in chloroform at room temperature, respectively.

The UV−vis absorption spectra (Figure 1) show maxima in two separated regions (see Table 1 for numerical values). Both the position and intensity of the bands strongly depend on the structure of the molecules. Parent compound **B1** exhibits intense absorption in two regions, approximately 250−290 and 290−390 nm, with very similar intensities. In general, the shape of the absorption spectrum, the position of its maximum, and its intensity are modified when increasing the π-conjugation between the difluoroboranyl unit and the electron-donor group.

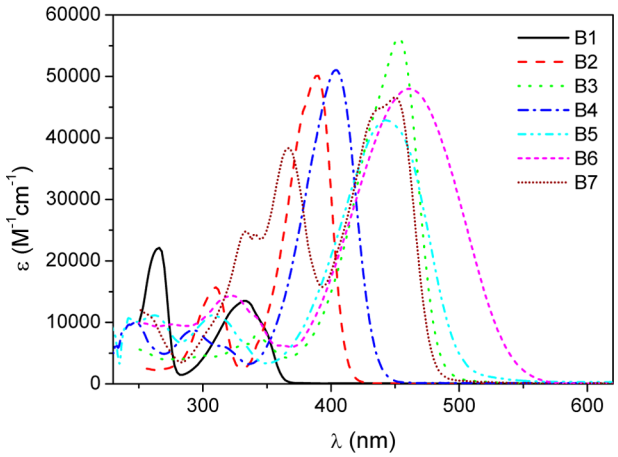

Figure 1. Electronic absorption spectra of compounds **B1**−**B7**.

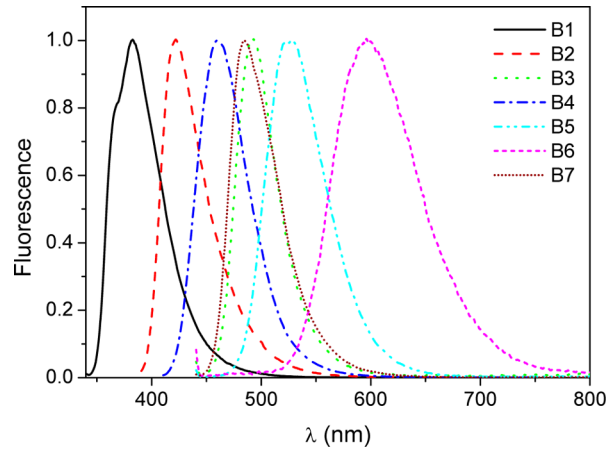

Figure 2. Normalized fluorescence spectra of compounds **B1**−**B7**.

DOI: 10.1021/acs.joc.5b02691
J. Org. Chem. 2016, 81, 2280−2292

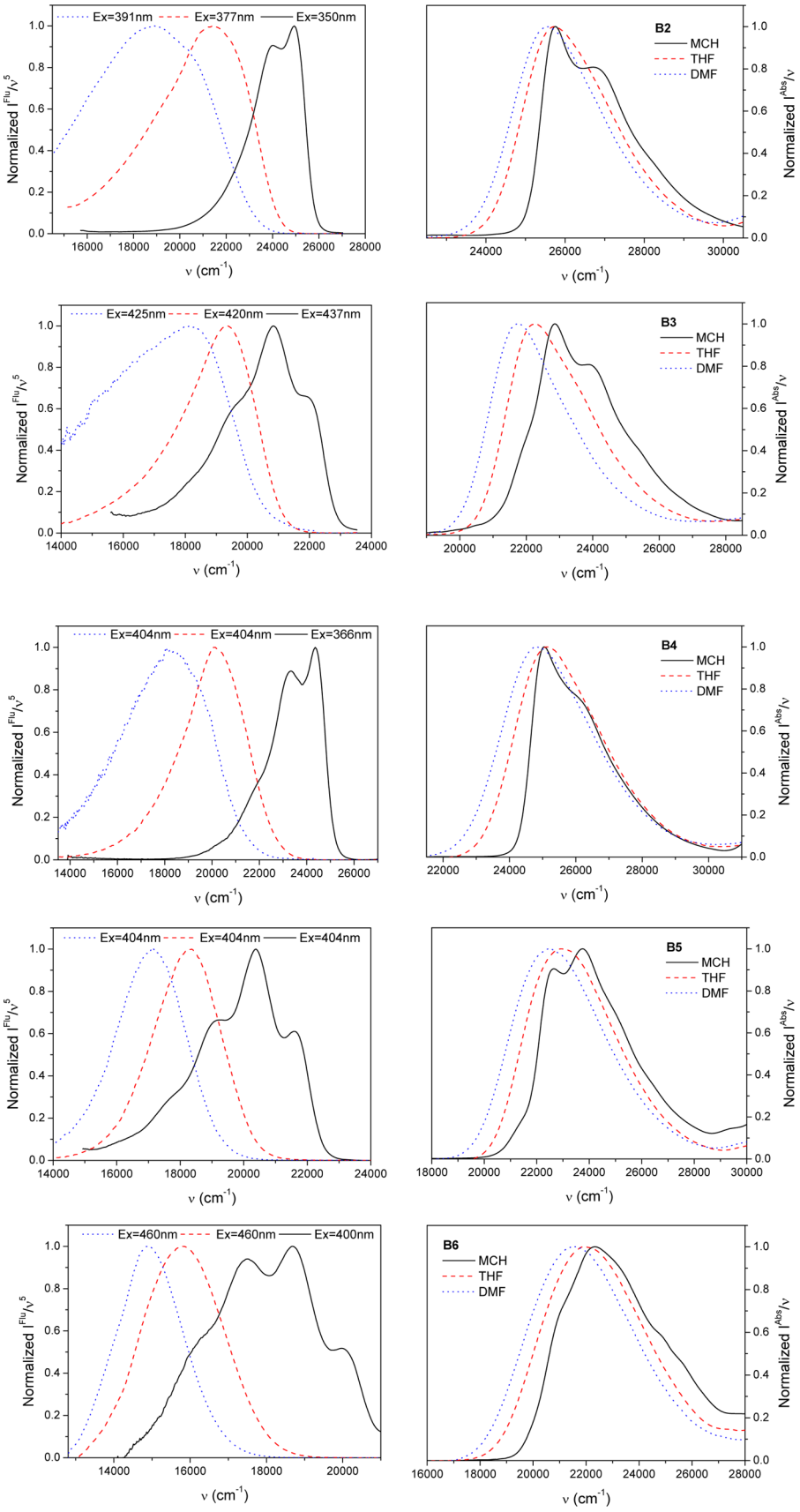

Figure 3. Scaled and normalized steady-state absorption (right panel) and fluorescence (left panel) spectra of the studied compounds in MCH, THF, and DMF.

DOI: 10.1021/acs.joc.5b02691
J. Org. Chem. 2016, 81, 2280−2292

Indeed, increasing the separation between the *N*,*N*-dimethylamine group and the BF_2 moiety by adding methine groups shifts the absorption band toward longer wavelengths, as expected. This effect is even more pronounced for the series of dyes encompassing a phenylene unit. In general, the introduction of an efficient π-conjugated spacer between the electron donor and the electron acceptor facilitates the electronic flow and enhances ICT, at least when the linker is relatively short. Comparing compounds presenting a similar conjugation path, it is noticeable that the branched compound **B7**, with a symmetrically substituted pyridine, presents a more red-shifted absorption compared to the asymmetric **B4** dye. This is a consequence of the cooperative ICT effects originating from the two arms.

Likewise, the fluorescence spectra shift toward longer wavelengths when the length of the π-conjugated path between the acceptor and the donor increases. The fluorescence intensity distribution of **B2**−**B7** in $CHCl_3$ is described by a classical Gaussian shape, which is characteristic for fluorescence spectra when the motions in the fluorophore environment occur simultaneously or faster than the emission. For these cases, a very large number of different solute-environment space configurations are possible, and their contributions give a broad emission band presenting a Gaussian topology.[60] In addition, the fluorescence intensity (quantum yield) decreases with increasing flexibility of the molecule, which is consistent with the presence of more radiationless deactivation paths in flexible derivatives. Indeed, the highest fluorescence quantum yields, calculated according to eq 1, were obtained for compounds **B1** and **B4**, whereas **B3** and **B6** are very weakly fluorescent (Table 1). We highlight that the introduction of a -CH═CH- moiety decreases ϕ_f by 32 and 50% (**B2** vs **B1** and **B5** vs **B4**), whereas a second addition of a -CH═CH- bridge causes the ϕ_f to lower by an additional 10%. The broadest fluorescence spectrum is observed for compound **B6** (Figure 2), and this is related to its intrinsic flexibility. An increase of the dimensionality of the molecule (**B7**) also decreases the fluorescence quantum yield (compared to **B4**) and the same holds for the Stokes shift. Similar trends have been observed in *N*,*N*-dimethylaminostyryl-substituted BODIPY.[3]

The Stokes shift ($\Delta\nu$, Table 1) changes regularly for compounds **B3**−**B6**. As can be seen in the Supporting Information (SI), the correlation between the number of π-electrons in the space separating the donor and BF_2 groups and the values of $\Delta\nu$ is high (linear correlation coefficient, *R*, attains 0.994). Inclusion of the Stokes shifts of **B1** and **B2** into the same correlation causes *R* to decrease to 0.952 (**B2** included) or 0.550 (both **B2** and **B1** included). This suggests that **B1** and to a much lesser extent **B2** are specific structures, probably due to their very small sizes and/or to a more limited rotation of the NMe_2 group in the ground-state. This limitation may be caused by charge polarization and partial double character of the CN bond and is seen in the ^{1}H NMR spectra giving two signals for CH_3 groups in **B1** and **B2** as in the DMF molecule. The same is seen in ^{13}C NMR spectra for **B1** and **B2**.

The fluorescence lifetimes of the fluoroboranyls in chloroform were determined from their emission decays described by the two-exponential fit. The fast decay lifetime of the compounds ranges from 50 to 700 ps and might be attributed to fluorescence from the nonrelaxed excited state, whereas the relaxed excited state is responsible for the nanosecond fluorescence lifetime. In the **B1**−**B3** series, τ_1 does not exhibit correlation with the number of π-electrons involved in conjugation, whereas in the **B4**−**B6** series, the linear correlation coefficient attains 0.993. Also, high correlation coefficients were found for τ_2 in **B1**−**B3** and **B4**−**B6** series (R = 0.953 and 0.959, respectively).

The fluorescence lifetimes (τ_1 and τ_2) and quantum yields were applied to calculate the radiative k_r and nonradiative k_{nr} rate constants.[61] Knowing the experimental values of the fluorescence quantum yield of the investigated fluorophores based on their decomposed fluorescence spectra (see Figure S3), we were able to estimate the intensity of the two separated bands and next calculate the radiative and nonradiative transition rate constants. It was found that for the rigid molecule **B1** the nonradiative transition rate is approximately twice that of the radiative rate. The increase of the size of the molecules by an increase of the π-conjugated path decreases the radiative rate constant k_r. We reasoned that the presence of methine groups provides additional degrees of freedom to the difluoroboranyls, which is likely the source of more efficient nonradiative transitions. It is interesting that, at first glance, the introduction of first and second -CH═CH- groups in **B1** (yielding **B2** and next **B3**, respectively) causes a decrease of $\Delta\nu$, whereas the same extension increases $\Delta\nu$ in the **B4**−**B6** series.

To clarify the role of solvent polarity in modifying both the ground and excited states properties of the molecules, we recorded the absorption and emission characteristic of the **B2**−**B6** compounds in methylcyclohexane (MCH), tetrahydrofuran (THF), and *N*,*N*-dimethylformamide (DMF) (Figure 3).

The tested compounds are sensitive to changes in solvent conditions, such as polarity, viscosity, and temperature. The absorption spectra are hardly affected by the polarity of the solvent, though the maximum is slightly red-shifted when the solvent is changed from MCH to DMF. The smallest solvent effect was observed for **B2**. Its absorption band with maxima at 388 nm in MCH shifts to 391 nm in DMF. The bathochromic shift caused by the solvent increases with an elongation of the π-conjugated system separating the electron-donor and the electron-acceptor moieties. The absorption band of **B6** moved from 446 nm in MCH to 460 nm in DMF. The same trend was observed in the fluorescence spectra but with much more pronounced effects. The fluorescence band shows a shift of ∼81 nm for **B2** and ∼128 nm for **B6** on changing the solvent from MCH to DMF, indicating the expected greater stabilization of the excited singlet state in polar solvents. Following the transition, the solvent dipoles can reorient or relax according to the polarity of the excited molecule, and this results in a lowering of the energy of the excited state.[61] The observed positive solvatochromic behavior is typical of compounds having enlarged dipole moments and CT character in that state (see below for the computed changes in dipole moment between the two states).[60,62] Additionally, the increase of solvent polarity results in loss of the structured emission, which is replaced by a longer-wavelength unstructured emission.

To some extent, the absorption and the emission spectra display a mirror-image shape, suggesting a relatively limited geometrical relaxation of Franck−Condon singlet excited state. More pronounced disruption of mirror symmetry is observed for **B2** and **B3** in DMF and **B5** and **B6** in MCH. Additionally, as illustrated in the right panel of Figure 3, only a single fluorescence band is observed for molecules dissolved in $CHCl_3$, and the location of the fluorescence peak remains invariant on λ_{Ex}. From Figure S4, it is also seen that the steady-state fluorescence excitation spectra of the compounds are not dependent on the observation wavelength. The fluorescence

DOI: 10.1021/acs.joc.5b02691
J. Org. Chem. 2016, 81, 2280−2292

Table 2. Fluorescence Lifetime (τ; ns) and Its Amplitude (α; %) for Compounds B2−B6 in MCH, THF, and DMF[a]

	MCH		THF		DMF	
no.	τ_1, α_1	τ_2, α_2	τ_1, α_1	τ_2, α_2	τ_1, α_1	τ_2, α_2
B2	0.167, 98.32	0.889, 1.68	0.469, 3.85	2.669, 96.15	0.299, 18.3	0.604, 81.7
B3	0.146, 83.67	1.492, 16.33	0.299, 31.23	0.760, 68.77	0.021, 97.12	0.940, 2.88
B4	0.506, 10.79	1.547, 89.21	0.420, 3.13	2.743, 96.87	0.351, 97.87	1.151, 2.13
B5	0.121, 98.18	1.217, 1.82	0.457, 9.32	1.657, 90.68	0.416, 16.19	1.000, 83.81
B6	0.073, 99.94	1.416, 0.06	0.414, 17.22	1.105, 82.78	0.433, 6.53	1.585, 93.47

[a]Correlation coefficient, χ^2, is 1.0−1.9%.

excitation spectra were recorded for three emission wavelengths (detection at the wavelength of the fluorescence maximum and both sides of the emission spectrum). As can be seen in Figure S4, the fluorescence excitation and absorption spectra are superimposable for compounds under study. In short, these results indicate that the emission occurs without significant changes in the spatial conformation of the molecules.

Besides the absorption and fluorescence spectra, the fluorescence decay lifetimes were also determined in MCH, THF, and DMF. The calculated fluorescence decay time data, τ_i, and the preexponential factors, α_i, describing the contribution of the ith fluorescence decay component of the total emission are compiled in Table 2.

One main feature arises from the data presented in Table 2. In nonpolar MCH, the picosecond fluorescence lifetime (τ_1) is the major decay component. With increasing solvent polarity, the contribution of the fast fluorescence decay component of the total emission decreases. This is accompanied by a rise in the percentage of the slow decay component (τ_1). **B4** is the only compound with the opposite effect, but this molecule differs in its structure from the other compounds under study. We can speculate that the fast decay component originates from the nonrelaxed ICT state, whereas the slow decay component results from the relaxed ICT state. This supposition is also reflected in the temperature effect on the position of the fluorescence spectra and their lifetimes. For all tested compounds, bathochromic shift of the emission maxima with decreasing temperature (see Table S1) was observed. As the π-conjugation between the difluoroboranyl unit and the *N*,*N*-dimethylamino group increases, the red shift becomes more significant (Figure S5). According to Lakowicz,[60] although solvent relaxation usually proceeds faster at higher temperatures, high temperature can also prevent the alignment of solvent dipoles. In general, the most pronounced red shifts occur at temperatures at which the solvent is fluid enough to reorient prior to emission but thermal energy is not so great as to disrupt these orientations.[60] Figure 4 shows the fluorescence decays of **B6** at different temperatures. The fluorescence lifetime of this large compound is found to be very sensitive to temperature. Indeed, from Figure 4 it is clear that the fluorescence lifetimes decrease with decreasing temperature of the solution.

Quantum-Mechanical Calculations. Theoretical calculations were performed to obtain complementary insights into the nature of the excited-states. First, for **B2**, **B3**, **B5**, and **B6**, both *Z* and *E* forms were investigated (see Table 3 for representation). The computed Gibbs energy is within ∼1 kcal/mol, such that these isomers most probably coexist in solution, and both were investigated in the following. For all compounds, theory predicts that the lowest-lying $\pi \rightarrow \pi^*$ transitions (associated with the absorption band of interest) are characterized by moderately large oscillator strengths (except

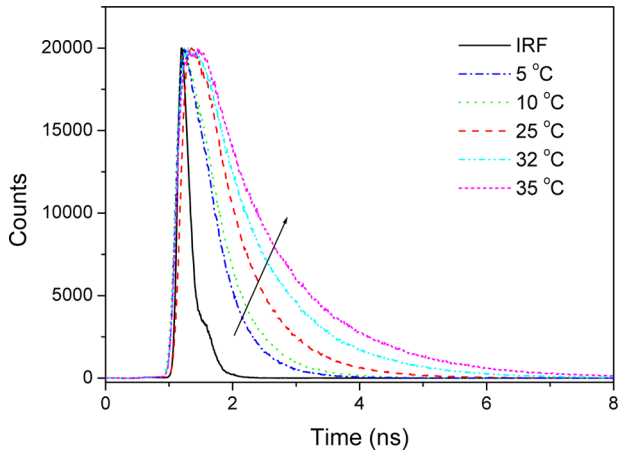

Figure 4. Fluorescence decay curves of **B6** in $CHCl_3$ recorded at different temperatures. λ_{ex} = 375 nm, λ_{em} = 620 nm. IRF = instrument response function.

of those for **B1**, for which the oscillator strength is small, in agreement with experimental data). As expected, the largest contribution to this band originates from HOMO → LUMO excitations, though non-negligible contributions from other orbitals are also present. For this reason, we have relied on density difference plots to analyze the nature of the relevant excited states. From the results shown in Table 3, it is clear that, upon photon absorption, charge is being transferred from the NMe_2 group (donor) to the ring containing the BF_2 moiety (acceptor). The phenyl ring present in systems **B4**−**B6** is acting as a secondary donor. This confirms the ICT nature of the transitions, though it is rather moderate for **B1**. It is worth noting that in **B1** the charge is transferred mainly to the pyridine ring, whereas in **B3**−**B6**, it is transferred mainly to the BF_2-carrying ring. In **B2**, both of these rings play a role (density difference plots, Table 3). Increasing distance between D and A, by adding vinyl and/or phenylene spacer(s), greatly improves the ICT distance that goes from 1.52 Å in **B1** to 4.46 Å in **B6**, whereas the amount of transferred charge, q_{CT}, remains unaffected. In the case of *Z* conformers, the d_{CT} values are ∼0.4 Å larger than their *E* counterparts, whereas q_{CT} remains unchanged. These two effects indicate that the difference between the excited-state and ground-state dipole moments are also steadily increasing in the series (see $\Delta\mu_{CT}$ in Table 3). The $\Delta\mu_{CT}$ are large for all compounds (except **B1**), which is consistent with the experimental results described above.

As stated in the Experimental Section, we have searched for the possibility of twisted ICT states by investigating the possible excited-state rotation of the terminal amino group and phenyl ring, but no minima could be found, indicating that only planar-like ICT excited state can emit in the present series.

DOI: 10.1021/acs.joc.5b02691
J. Org. Chem. 2016, 81, 2280−2292

Table 3. Density Difference Plots and CT Parameters Determined at the M06-2X Level (see Experimental Section for Details)

	Density difference plot	d_{CT} [Å]	q_{CT} [e]	$\Delta\mu_{CT}$ [D]
B1	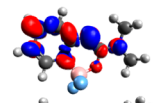	1.52	0.50	1.33
B2 (*Z*)	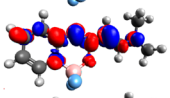	2.14	0.54	4.79
B2 (*E*)	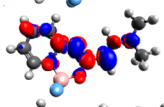	1.77	0.52	2.94
B3 (*Z*)	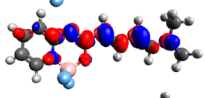	3.04	0.56	7.75
B3 (*E*)	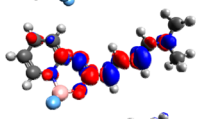	2.61	0.54	5.36
B4	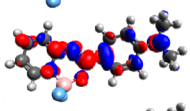	3.38	0.65	8.15
B5 (*Z*)	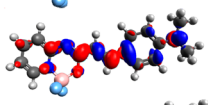	4.10	0.65	11.03
B5 (*E*)	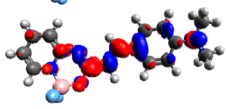	3.72	0.63	9.53
B6 (*Z*)	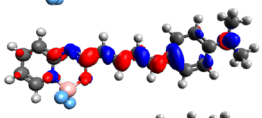	4.79	0.66	13.62
B6 (*E*)	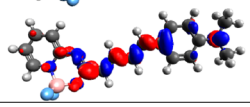	4.46	0.64	12.13

Consistent with the increase of the ICT nature of the first transition, theory predicts substantial bathochromic shifts when going from **B1** to **B2** and **B3** or from **B4** to **B5** and **B6** (Table 4). Within the vertical approximation, theory slightly underestimates the λ_{abs} as well as λ_{em} wavelengths, i.e., it overshoots the transition energies. In Table 4 and Figure 5, one can find the absorption/fluorescence crossing point (AFCP) values, which can be more rigorously compared to the experimental data. For these energies, the deviations from experiment vary from 2 nm (**B1**) to 53 nm (**B6**). This larger discrepancy compared to experimental data for the biggest system could result from the enhanced ICT nature of the excited state in **B6**. Moreover, **B5** and **B6** are characterized by significant Stokes shifts, up to 5310 and 6342 cm^{-1} (depending on conformation), indicating that the excited-state structures significantly differ from their ground-state counterparts. The $\Delta\nu$ values are higher for **B1**, **B5**, and **B6** in experiments as well as in theory, although quantum mechanics overshoots the $\Delta\nu$. It is worth noting that the predicted $\Delta\nu$ values are in line with experimental ones ($\Delta\nu_{exp} = a\ \Delta\nu_{theor} + b$, $R = 0.951$, $a = 1.03$, $b = 1252$) and that both depend on the number of π-electrons involved in the conjugation path. As for the experimental values (see above), a high correlation coefficient is obtained in the **B2**−**B6** series ($R = 0.971$), whereas **B1** substantially deviates from this relationship (see the SI).

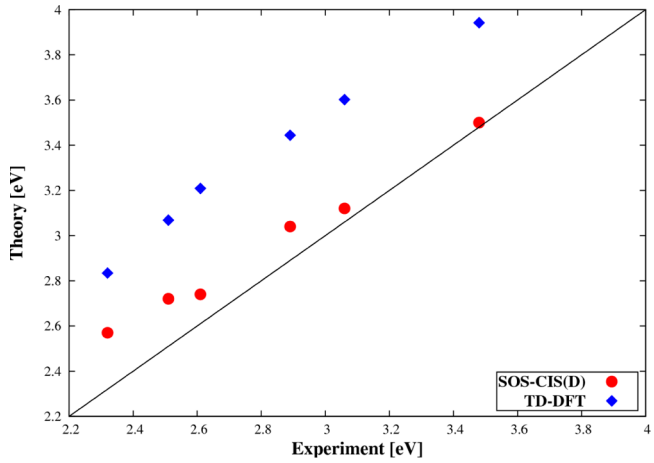

Figure 5. Comparison of the TD-DFT, SOS-CIS(D), and experimental AFCP values for the difluoroboranyl dyes **B1**−**B6**. The central line indicates a perfect theory−experiment match.

The SOS-CIS(D) results indicate, consistently with measurements, that extending the length of the π-conjugation path results in bathochromic shifts. More specifically, theoretical calculations indicate that the series without a phenyl ring is characterized by substantial absorption bathochromic shifts relative to **B1** (**B2** + 51 nm and **B3** + 90 nm), whereas the predicted shifts are smaller for the systems with the phenylene spacer (**B5** + 25 nm, **B6** + 36 nm compared to **B4**). As was

Table 4. Experimental and Calculated Spectroscopic Parameters Corresponding to the Lowest Lying ($\pi \rightarrow \pi^*$) Excited State[a]

	experiment				theory			
	λ_{abs} [nm]	λ_{em} [nm]	$\Delta\nu$ [cm^{-1}]	AFCP [nm]	λ_{abs} [nm]	λ_{em} [nm]	$\Delta\nu$ [cm^{-1}]	AFCP [nm]
B1	334.5	382.0	3717	356.0	308.5	366.8	5147	354
B2 (*Z*)	389.5	421.0	1921	405.6	358.3	397.2	2737	396
B2 (*E*)	389.5	421.0	1921	405.6	359.0	399.8	2842	398
B3 (*Z*)	454.5	492.0	1677	475.0	397.7	459.7	3302	448
B3 (*E*)	454.5	492.0	1677	475.0	398.9	464.3	3535	452
B4	404.0	459.0	2966	429.5	365.0	423.3	3770	408
B5 (*Z*)	441.5	527.0	3675	493.5	388.7	486.1	5156	452
B5 (*E*)	441.5	527.0	3675	493.5	390.4	492.5	5310	456
B6 (*Z*)	460.5	595.0	4929	538.0	398.8	532.8	6303	480
B6 (*E*)	460.5	595.7	4929	538.0	401.1	538.0	6343	483

[a]For the theoretical part, accounting for SOS-CIS(D) corrections, the λ_{abs} and λ_{em} are determined in the vertical approximation, and $\Delta\nu$ is the Stokes shift.

DOI: 10.1021/acs.joc.5b02691
J. Org. Chem. 2016, 81, 2280−2292

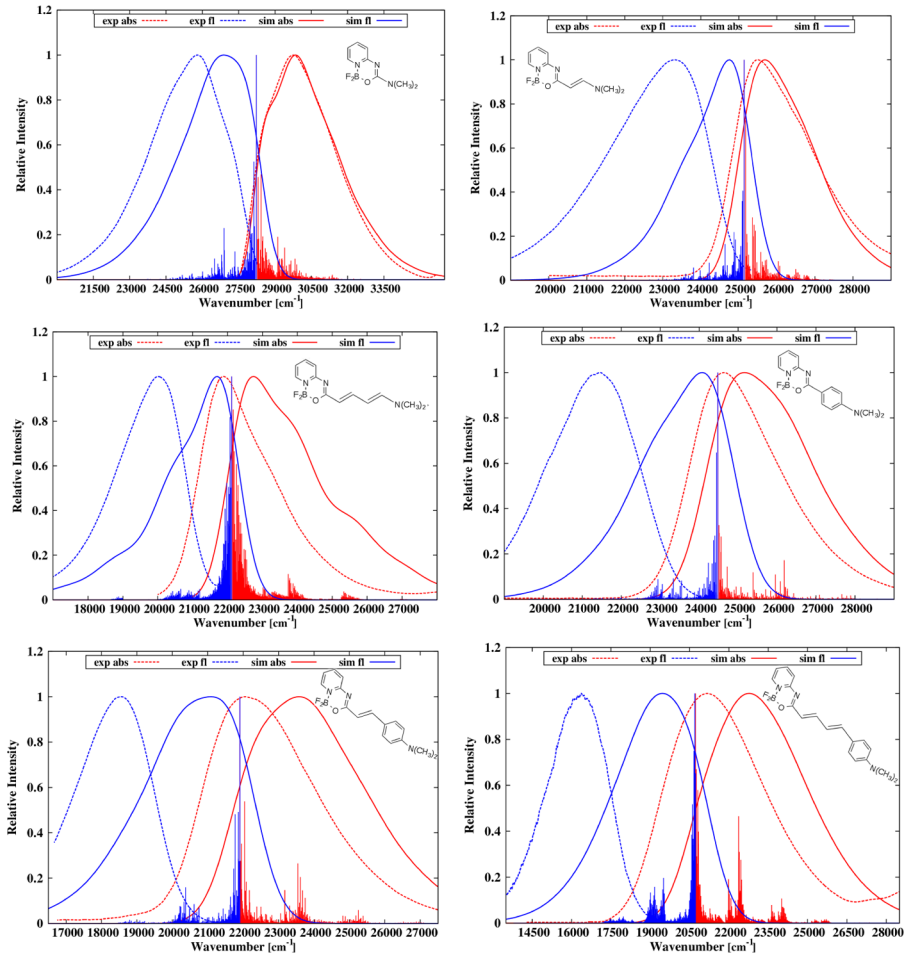

Figure 6. Comparison of experimental and theoretical (both stick and convoluted) spectra for **B1**−**B6**. For comparison issues, the experimental spectra were transformed from nm to cm^{-1}, rescaled (I_{abs}/υ^3 and I_{em}/υ^5) and then normalized to obtain line shapes. For the longer systems, only the *E* isomers are shown.

mentioned, the same tendencies can be easily found in corresponding experimental data: going from **B1** to **B2** and to **B3** results in +55 and +120 nm shifts, whereas for **B4** to **B5** and to **B6**, it is only +37.5 and +56.5 nm, respectively. Opposite trends are obtained for the emission calculations with larger shifts determined for the second series of compounds (**B5** + 69 nm, **B6** + 115 nm, whereas **B2** + 33 nm, **B3** + 98 nm). These results also remain in line with the measurements because the shifts of the fluorescence wavelengths are equal to +68 and +136 nm when going from **B4** to **B5** and to **B6** and +39 and +110 nm when going from **B1** to **B2** and to **B3**, respectively (see Table 3).

We also highlight that the calculated solvent reorganization energies (within the range of 0.0128 eV in **B1** up to 0.0558 eV for **B6**) are globally following the trends of the full width at half maximum (fwhm) values obtained from experimental absorption spectra (2386−4408 cm^{-1}). It is indeed expected that larger solvent reorganization energies correlate with broader absorption bands. More interestingly, these reorganization energies grant useful hints for determining the fwhm values used in vibrationally resolved spectra computations (see below): the larger the reorganization energy, the larger the fwhm used.

We also used theoretical calculations to determine vibronic couplings and hence compare simulated band shapes to the experimental data. As can be seen in Figure 6, theory satisfactorily reproduces the vibrational fine structure of the absorption band that corresponds to the $\pi \rightarrow \pi^*$ transition for all compounds. In the case of emission, the predicted spectra are a bit too broad compared to experiment, especially for the most expanded compounds (**B5** and **B6**). As stated above, the broadening function used was proportional to the computed solvent reorganization energies.

Consistent with Figure 5, one finds in Figure 6 rather limited discrepancies between the experimental and theoretical positions of the bands maxima and reasonably reproduced successive red shifts (going from **B1** to **B6**). A general trend however is that the optical spectra (both absorption and emission) are more accurate for smaller systems. For the expanded systems (**B3**, **B5**, **B6**), the number of low-intensity sticks contributing to the vibronic spectra is significantly larger than in the other compounds, consistent with the higher flexibility of these compounds. Indeed, this indicates significant contributions of many low-frequency modes that are often less accurately reproduced in the harmonic approximation.

To gain insights into the origins of specific band shapes, we identified the key vibronic contributions for all structures. This analysis revealed that each structure has a specific set of vibrational modes mainly responsible for spectra shape (see Table 5). In the case of the compact systems (**B1** and **B4**), the most intense modes were N−B stretching combined with asymmetric C−H bending localized in the ring next to the BF_2

DOI: 10.1021/acs.joc.5b02691
J. Org. Chem. 2016, 81, 2280−2292

Table 5. Vibronic Analysis of the Vibrational Mode Contributing the Most to High-Energy Vibronic Couplings[a]

	Absorption Vibrational mode	Freq [cm^{-1}] Int	Emission Vibrational mode	Freq [cm^{-1}]
B1	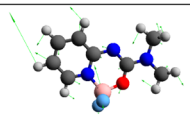	1166.7 0.0108	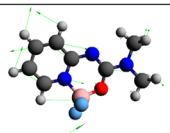	1730.5 0.0872
B2	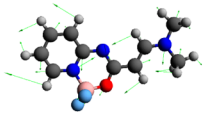	1355.0 0.0080	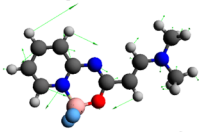	1331.0 0.0888
B3	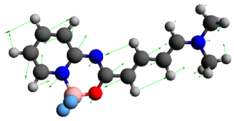	1623.2 0.0034	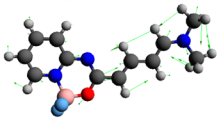	1455.7 0.0108
B4	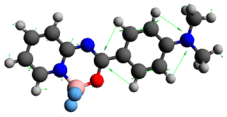	1704.5 0.0307	*Coupling of 2 modes*	1570.6 0.0994
B5	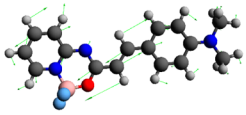	1637.6 0.0179	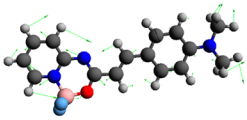	1533.3 0.0798
B6	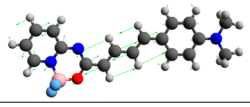	1642.7 0.0086	*Coupling of 2 modes*	1219.6 0.0368

[a]Note that only the *E* conformers were considered consistently with Figure 6.

moiety and C−H asymmetric bending combined with C−C stretching originating from the phenyl ring, respectively. For the expanded systems with double bonds (**B2**, **B3**, **B5**, and **B6**), crucial modes consist of the combination of asymmetric C−H bending in the phenyl ring attached to the BF_2-containing ring and asymmetric C−C stretching of the double bond(s). Additionally, for expanded systems, many contributions from combination modes also play a role.

Finally, we give the theoretical results obtained for **B7** in Tables 6−8 as well as in Figure 7. Looking at Table 6, one can see that, in contrast to systems discussed above, the reorganization of the density in **B7** is mainly located in the central part of the structure, though the donating character of the NMe_2 groups pertains. As expected for a symmetric molecule, the dipolar charge-transfer distance is rather small due to the opposite local dipoles of the two amino groups.

Table 6. Density Difference Plots and ICT Parameters for B7

	Density difference plot	d_{CT} [Å]	q_{CT} [e]	$\Delta\mu$ [D]
B7	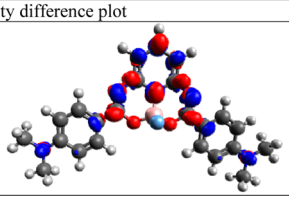	1.20	0.59	3.04

Table 7. Experimental and Calculated Spectroscopic Parameters Corresponding to the Lowest Lying ($\pi \rightarrow \pi^*$) Excited State in B7[a]

	experiment				theory			
	λ_{abs} [nm]	λ_{em} [nm]	$\Delta\nu$ [cm^{-1}]	AFCP [nm]	λ_{abs} [nm]	λ_{em} [nm]	$\Delta\nu$ [cm^{-1}]	AFCP [nm]
B7	452	487	1590	471	410	474	3306	460

[a]For the theoretical part, that includes a SOS-CIS(D) correction, the λ_{abs} and λ_{em} are determined in the vertical approximation, and $\Delta\nu$ is the Stokes shift.

The SOS-CIS(D) predictions for **B7** are similar to those for extended systems described above, and the AFCP value is predicted with 10 nm accuracy. Vibrationally resolved absorption and emission bands for dye **B7** are presented in Figure 7, and Table 7 demonstrates that the used methodology is able to satisfactorily reproduce the optical signature even for the large molecule (**B7**). As expected, in line with the symmetry group, the most intense modes for absorption and emission correspond to symmetric vibrations, principally C−H scissoring and C−N stretching of the central ring (see Table 8).

■ CONCLUSIONS AND OUTLOOK

In this work, we have synthesized and thoroughly characterized seven new difluoroboranyls. All are characterized by dimethylamine donors separated from the fluoroboranyl center by vinyl and/or phenylene spacers of different lengths. The experimental investigation of their optical properties showed that increasing the π-conjugation length leads to (i) a bathochromic displacement of the absorption and emission bands, (ii) a decrease of the fluorescence quantum yields, (iii) an increase of the Stokes shifts, and (iv) a broadening of the bands. Except for the shortest compound (**B1**) that behaves differently, these trends were systematically found in the investigated series. First-principle calculations were used to model these compounds. Besides a generally reasonable agreement between theory and experiment for both the position and shape of the

DOI: 10.1021/acs.joc.5b02691
J. Org. Chem. 2016, 81, 2280−2292

Table 8. Vibronic Analysis of the Most Intense (High-Wavelength) Components

	Absorption			Emission		
	Vibrational mode	Freq [cm^{-1}]	Int	Vibrational mode	Freq [cm^{-1}]	Int
B7	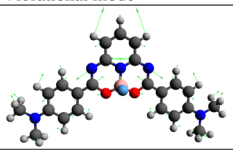	1509.4	0.0278	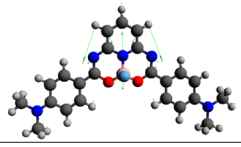	1146.5	0.0808

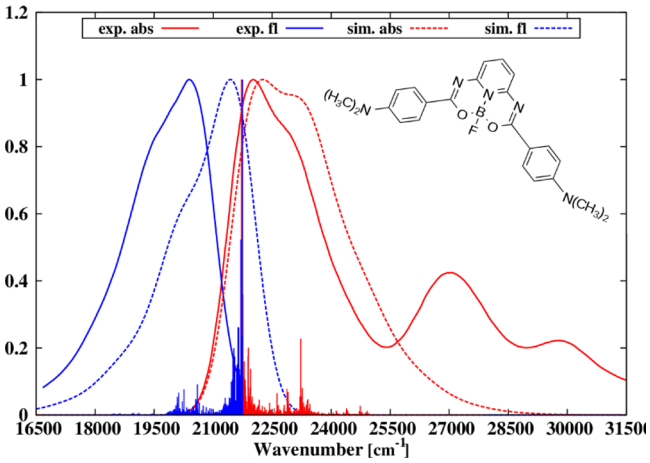

Figure 7. Comparison of experimental and theoretical spectra **B7**.

absorption and emission bands, the theoretical calculations have highlighted the presence of a strong ICT that is steadily enhanced when the distance between the amino donor and the difluoroboranyl moiety, acting as an acceptor, increases. They also demonstrated that the phenylene ring attached to the donor group acts as a secondary donor in these compounds. The broader optical spectra obtained for the largest compounds could be explained, on the one hand, by the larger solvent reorganization energies found in these systems, and on the other hand, by the fact that vibronic couplings include more low-frequency modes in the larger and more flexible derivatives. In turn, this enhanced flexibility explains the smaller emission quantum yields.

We are currently continuing our investigation of original fluorophores in which the difluoroboranyl group is tethered between different electronegative atoms.

■ EXPERIMENTAL SECTION

Synthesis. Scheme 2 shows the general synthesis path that we have followed.

Esters **2** and **4** were commercially available. The remaining esters were obtained as follows: **3** from methyl crotonate and bis-(dimethylamino)methoxymethane,[63] **5** in the Wittig olefination reaction of $Ph_3P{=}CHCO_2Et$ and 4-(dimethylamino)benzaldehyde according to published procedure,[64] and for the synthesis of **6**, 4-(dimethylamino)cinnamaldehyde, commercially available, was used to give the desired ester.[64] Wittig reagent used in said reactions was obtained from triphenylphosphine and ethyl bromoacetate according to a known procedure.[65] Compound **A1** was previously known and was obtained as described elsewhere.[66] Compound **A2** (as well as **A3**−**A6**) is new and was obtained by treating a THF solution (40 mL) of 2-aminopyridine (0.73 g, 7.7 mmol) with NaH (60% suspension in oil, 2 M excess with respect to the number of amino groups, 0.62 g) and then with the respective ester (equimolar amount) according to published synthetic route.[38] The mixture was refluxed for 24 h, and then after cooling to rt, 0.84 g of NH_4Cl in 20 mL of water was added, mixed at rt for 2 h, and evaporated to give a suspension in water, which was extracted with chloroform (3 × 50 mL). Extracts were dried with Na_2SO_4 and evaporated, and residual solid was recrystallized from alcohol. The remaining amides were obtained analogously. The synthesis of compounds **B1**−**B6** were performed by treating heterocyclic amides (**A1**−**A6**) with BF_3 etherate in the presence of DIEA.[38] The solution of amide **A1** (0.50 g) in dry DMC was treated with BF_3 etherate (2 mL) and DIEA (5 mL) and stirred magnetically for 24 h. Then, the saturated Na_2CO_3 solution was added (20 mL), stirred for 2 h, and extracted with DCM, and the organic layer was dried with Na_2SO_4 and evaporated. Fluoroboranyl **B7** was obtained by heating **A7** (0.64g, 1.6 mmol) with BF_3 etherate (2.0 mL) in boiling, dry toluene (20 mL) overnight.[67] After that time, the solution was evaporated. Compounds **B1**−**B7** were purified by column chromatography using SiO_2 and DCM as an eluent.

The NMR spectra were recorded in perdeuterated dimethyl sulfoxide (DMSO-d_6) or chloroform ($CDCl_3$) using a ^{1}H (400 MHz) and ^{13}C (100 MHz) spectrometer. All chemical shifts are quoted in ppm relative to tetramethylsilane (TMS) using the residual solvent peak as a reference standard (DMSO-d_6: ∼2.49 ppm ^{1}H;

Scheme 2. Synthesis of Bifluoroboranyl Compounds B1−B7

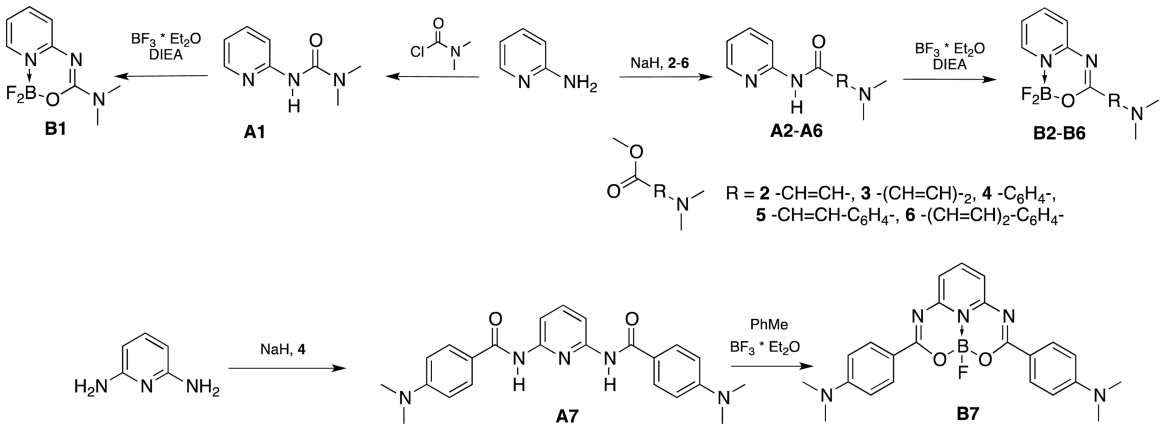

DOI: 10.1021/acs.joc.5b02691
J. Org. Chem. 2016, 81, 2280−2292

~39.5 ppm ^{13}C, and $CDCl_3$: ~7.24 ppm ^{1}H; ~77.0 ppm ^{13}C). Coupling constants (J) were reported in Hertz.

Photophysical Measurements. The steady-state electronic absorption and fluorescence spectra were recorded at room temperature. The slit width was 5 nm for both excitation and emission. The concentration of difluoroboranyls in chloroform was 1.0×10^{-5} and 1.0×10^{-6} M for absorption and emission measurements, respectively. The relative fluorescence quantum yields of the difluoroboranyls were obtained by comparing the area under the corrected emission spectrum of the tested sample (A ≈ 0.1 at an excitation wavelength) with that of a solution of 9,10-diphenylantracene in cyclohexane (λ_{Ex} = 335 or 380 nm; ϕ_{ref} = 0.90−0.93) and Coumarin 153 in ethanol (λ_{Ex} = 420 nm; ϕ_{ref} = 0.38).[68] The quantum yield of the tested dyes (ϕ_s) was calculated using eq 1.

$$\phi_s = \phi_{ref} \frac{I_s A_{ref}}{I_{ref} A_s} \cdot \frac{n_s^2}{n_{ref}^2} \quad (1)$$

where ϕ_{ref} is the fluorescence quantum yield of reference sample, A_s and A_{ref} are the absorbances of the difluoroboranyl and reference samples at the excitation wavelengths, I_s and I_{ref} are the integrated emission intensities for the difluoroboranyl and reference samples, and n_s and n_{ref} are the refractive indices of the solvents used for the difluoroboranyl and the reference, respectively. The fluorescence lifetimes were measured using a single-photon counting system. The apparatus uses a picosecond diode laser for the excitation, generating pulses of approximately 81.5 ps at 466.6 nm or 55 ps at 375 nm. Its maximal average power is 5 mW. Short laser pulses in combination with a fast microchannel plate photodetector and ultrafast electronics allow analysis of fluorescence decay signals in the range down to single picoseconds. The dyes were studied at the concentration at which they exhibit similar absorbance at an excitation wavelength (~0.1 in a 10 mm cell). The fluorescence decays were fitted to two-exponential functions.

Quantum-Mechanical Calculations. The computational protocol follows the one described previously for reproducing band shapes and optical signatures of fluoroborates,[69,70] and it is therefore only briefly summarized here. All DFT and TD-DFT were performed using the latest version of the Gaussian 09[71] program package, applying a tightened self-consistent field convergence criterion (10^{-9}−10^{-10} au) and an improved optimization threshold (10^{-5} au on average residual forces). In all DFT and TD-DFT calculations, the so-called *ultrafine* pruned (99,590) integration grid was applied. The SOS-MP2 and SOS-CIS(D) calculations have been determined with the Q-Chem package[72] using the resolution of identity (RI) scheme.

First, the geometrical and vibrational parameters of the ground-state were determined with DFT and the 6-31G(d) atomic basis set. This basis set has been shown to provide accurate structures for BODIPY-like compounds.[70,73] Next, the same parameters have been obtained for the first excited-state using TD-DFT and the same atomic basis set. Of course, all structures presented here correspond to true minima of the potential energy surface (no imaginary frequencies). We checked the absence of possible multiple minima in the excited-state using relaxed scans considering key flexible dihedral angles, and no stable TICT-like geometry was found. In a third step, the transition energies between the two states have been determined at the TD-DFT and SOS-CIS(D) levels of theory, both using the 6-311+G(2d,p) atomic basis set (and a triple-ζ auxiliary basis set for the RI part).[73] All of the DFT and TD-DFT calculations were carried out with the three different exchange-correlation functionals, namely M06-2X,[74] CAM-B3LYP,[75] and PBE0.[76] After tests, it turned out that the former was the most suited for our needs, consistently with previous investigations,[69,70] and we present only M06-2X data here. To take into account the conditions of experimental measurements, we carried out the DFT and TD-DFT calculations (geometry optimization, vibrational calculations, and transition energies) in the presence of the solvent (here: chloroform), using the polarizable continuum model (PCM)[77] in its corrected linear response (cLR) derivation for the excited-state energies.[78] All energies (vertical absorption, vertical emission, and 0−0 energies that can be directly compared to experimental absorption-emission crossing points) are obtained at the cLR-PCM-TD-DFT level and corrected by the difference between SOS-CIS(D) and TD-DFT gas-phase results. We redirect the readers to previous works for more details.[69,70] Excited-state reorganization energies were determined using a comparison of the nonequilibrium and equilibrium energies results.[79]

The density difference plots shown have been obtained at the PCM-TD-M06-2X/6-311+G(2d,p) level and are represented with a contour threshold of 0.002 au. In these graphs, the blue (red) zones indicate density decrease (increase) upon electronic transition. The charge-transfer parameters, namely, the charge-transfer distance, d_{CT}, and the amount of transferred charge, q_{CT}, have been determined following a procedure described elsewhere.[80,81] Vibrationally resolved spectra of fluoroboranyl complexes that present a specific band shape have been obtained using the FCclasses program[82−84] applying the Franck−Condon (FC) approximation as strongly dipole-allowed ES are considered here. The reported spectra have been simulated using a convoluting Gaussian function presenting a full width at half-maximum that has been adjusted to allow accurate comparisons with experiments (typical value: 0.16 eV). A maximal number of 25 overtones for each mode and 20 combination bands on each pair of modes were included in the calculation. The maximum number of integrals to be computed for each class was, at most, set to 10^{12} to reach FC factors higher than 0.9 for all presented vibronic spectra. Note that comparisons between theoretical and experimental absorption and emission spectra use normalization procedures that allow for obtaining physically comparable line shapes.[85]

Compound Characterization. For some compounds, signal originating from the CH_3 group in ^{13}C spectra is not visible due to its overlap with solvent multiplets. However, the said signal is visible in ^{1}H, ^{13}C HSQC, or/and HMBC spectra.

*(E)-3-(Dimethylamino)-N-(pyridin-2-yl)acrylamide (**A2**).* Yield of 0.96 g (65%). Mp 171.2−174.2 °C (EtOH), light yellow powder. ^{1}H NMR (TMS, DMSO-d_6): δ 9.65 (s, 1H, NH), 8.21 (dd, 1H, CH), 8.15 (d, 1H, CH, J = 8.4 Hz), 7.65 (dt, 1H, CH, J = 7.8, 1.8 Hz), 7.37 (d, 1H, CH, J = 12.7 Hz), 6.93 (ddd, 1H, CH, J = 7.4, 5.7, 1.0 Hz), 4.95 (d, 1H, CH, J = 12.6 Hz), 2.86 (s, 6H, CH_3). ^{13}C (TMS, DMSO-d_6): δ 167.3, 153.9, 151.5, 148.1, 18.0, 118.1, 113.4, 88.3, CH_3 overleaped by the solvent. ^{15}N ($MeNO_2$, $CDCl_3$): δ −300.8, −238.9, −94.2. Anal. Calcd for $C_{10}H_{13}N_3O$: C 62.81, H 6.85, N 21.97. Found: C 62.73, H 6.93, N 21.78.

*(2E,4E)-5-(Dimethylamino)-N-(pyridin-2-yl)penta-2,4-dienamide (**A3**).* Yield of 0.88 g (62%). Mp 113.3−115.2 °C (EtOH), light orange crystalline. ^{1}H NMR (TMS, DMSO-d_6): δ 10.00 (s, 1H, NH), 8.24 (dd, 1H, CH), 8.19 (d, 1H, CH, J = 8.4 Hz), 7.70 (dt, 1H, CH, J = 7.8, 2.0 Hz), 7.26 (dd, 1H, CH, J = 14.2, 11.5), 6.99 (m, 1H, CH, overleaped), 6.95 (d, 1H, CH, 12.7 Hz), 5.78 (d, 1H, CH, J = 14.2 Hz), 5.07 (dd, 1H, CH, J = 12.8 Hz), 2.84 (s, 6H, CH_3). ^{13}C (TMS, DMSO-d_6): δ 166.6, 153.6, 151.8, 148.2, 145.4, 138.1, 118.6, 113.6, 109.6, 96.1, CH_3 overleaped by the solvent. ^{15}N ($MeNO_2$, $CDCl_3$): δ −302.0, −236.1, −92.9. Anal. Calcd for $C_{12}H_{15}N_3O$: C 66.34, H 6.96, N 19.34. Found: C 66.26, H 7.02, N 19.20.

*4-(Dimethylamino)-N-(pyridin-2-yl)benzamide (**A4**).* Yield of 1.60 g (70%). Mp 145.4−146.9 °C (EtOH), cream-colored powder. ^{1}H NMR (TMS, $CDCl_3$): δ 8.78 (bs, 1H, NH), 8.45 (d, 1H, CH, J = 8.4 Hz), 8.28 (m, 1H, CH), 7.88 (d, 2H, CH, J = 9.0 Hz), 7.78 (dt, 1H, CH, J = 7.9, 1.9 Hz), 7.06 (ddd, 1H, CH, J = 7.5, 4.9, 0.9 Hz), 6.73 (d, 2H, CH, J = 9.0 Hz), 3.07 (s, 6H, CH_3). ^{13}C (TMS, $CDCl_3$): δ 165.5, 154.0, 152.0, 146.9, 138.9, 129.0, 120.3, 119.2, 114.3, 111.1, 40.1. ^{15}N ($MeNO_2$, $CDCl_3$): δ −322.3, −246.6, −105.6. Anal. Calcd for $C_{14}H_{15}N_3O$: C 69.69, H 6.27, N 17.41. Found: C 69.50, H 6.41, N 17.27.

*(E)-3-(4-(Dimethylamino)phenyl)-N-(pyridin-2-yl)acrylamide (**A5**).* Yield of 1.26 g (54%). Mp 155.2−158.0 °C (EtOH), yellow powder. ^{1}H NMR (TMS, $CDCl_3$): δ 8.79 (bs, 1H, NH), 8.40 (d, 1H, CH, $^3J_{H,H}$ = 8.4 Hz), 8.29 (dd, 1H, CH), 7.74 (t, 1H, CH), 7.72 (d, 1H, CH, J = 15.3 Hz), 7,43 (d, 2H, CH, J = 11.6 Hz), 7.05 (m, 1H, CH), 6.67 (d, 2H, CH, J = 11.6 Hz), 6.37 (d, 1H, CH, J = 15.4 Hz), 3.02 (s, 6H, CH_3). ^{13}C (TMS, $CDCl_3$): δ 165.3, 152.1, 151.7, 147.2, 143.7, 138.7, 129.8, 122.2, 119.3, 114.9, 114.5, 111.9, 40.1. ^{15}N

DOI: 10.1021/acs.joc.5b02691
J. Org. Chem. 2016, 81, 2280−2292

($MeNO_2$, $CDCl_3$): δ −323.7, −235.6, −102.6. Anal. Calcd for $C_{16}H_{17}N_3O$: C 71.89, H 6.41, N 15.72. Found: C 71.78, H 6.50, N 15.60.

*(2E,4E)-5-(4-(Dimethylamino)phenyl)-N-(pyridin-2-yl)penta-2,4-dienamide (**A6**).* Yield of 0.99 g (67%). Mp 190.8−191.8 °C (EtOH), orange powder. ^{1}H NMR (TMS, $CDCl_3$): δ 8.55 (bs, 1H, NH), 8.36 (d, 1H, CH, *J* = 8.4 Hz), 8.29 (m, 1H, CH), 7.72 (dt, 1H, CH, *J* = 7.8, 1.9 Hz), 7.55 (dd, 1H, CH, *J* = 14.6, 11 Hz), 7.36 (d, 2H, CH, *J* = 8.8 Hz), 7.03 (ddd, 1H, CH, *J* = 7.4, 4.9, 1.0 Hz), 6.86 (d, 1H, CH, *J* = 15.4 Hz), 6.71 (dd, 1H, CH, *J* = 15.6, 11.0 Hz), 6.66 (d, 2H, CH, *J* = 8.8 Hz), 6.01 (d, 1H, CH, *J* = 14.7 Hz), 3.00 (s, 6H, CH_3). ^{13}C (TMS, $CDCl_3$): δ 164.9, 152.0, 150.9, 147.7, 144.2, 141.4, 138.4, 130.8, 128.7, 124.2, 121.6, 120.6, 119.5, 114.3, 112.0, 40.2. ^{15}N ($MeNO_2$, $CDCl_3$): δ −325.6, −234.6, −97.8. Anal. Calcd for $C_{18}H_{19}N_3O$: C 73.69, H 6.53, N 14.32. Found: C 73.57, H 6.62, N 14.21.

*N,N′-(Pyridine-2,6-diyl)bis(4-(dimethylamino)benzamide) (**A7**).* Yield of 0.74 g (61%). Mp 223.4−226.0 °C (MeOH), light-brown crystals. ^{1}H NMR (TMS, DMSO-d_6): δ 9.97 (s, 2H, NH), 7.92 (d, 4H, CH, *J* = 9.0 Hz), 7.86−7.78 (m, 3H, CH, pyridine), 6.76 (d, 4H, CH, *J* = 9.0 Hz), 3.01 (s, 12H, CH_3). ^{13}C (TMS, DMSO-d_6): δ 165.6, 153.1, 151.3, 140.1, 129.8, 120.5, 111.3, 110.5, 49.1. Anal. Calcd for $C_{23}H_{25}N_5O_2$: C 68.47, H 6.25, N 17.36. Found: C 68.40, H 6.31, N 17.27.

*3-(Dimethylamino)-1,1-difluoro-1H-pyrido[1,2-c][1,3,5,2]-oxadiazaborinin-9-ium-1-uide (**B1**).* Yield of 0.27 g (42%). Mp 104.0−105.8 °C, white crystals. ^{1}H NMR (TMS, $CDCl_3$): δ 7.95 (m, 1H, CH), 7.70 (dt, 1H, CH, *J* = 7.8 Hz, 1.8 Hz), 6.99 (d, 1H, CH, J = 8.6 Hz), 6.87 (t, 1H, CH), 3.18 (s, 3H, CH_3), 3.12 (s, 3H, CH_3). ^{11}B ($BF_3{\cdot}Et_2O$, $CDCl_3$): δ 0.457 (t). ^{13}C (TMS, $CDCl_3$): δ 158.5, 156.6, 141.8, 137.0, 121.2, 114.9, 37.1, 36.0. ^{15}N ($MeNO_2$, $CDCl_3$): δ −295.3, −213.5, −186.8. ^{19}F ($CFCl_3$, $CDCl_3$): δ −142.6. Anal. Calcd for $C_8H_{10}BF_2N_3O$: C 45.11, H 4.73, N 19.73. Found: C 44.99, H 4.81, N 19.56.

*(E)-3-(2-(Dimethylamino)vinyl)-1,1-difluoro-1H-pyrido[1,2-c]-[1,3,5,2]oxadiazaborinin-9-ium-1-uide (**B2**).* Yield of 0.62 g (62%). Mp 179.6−181.9 °C, yellow powder. ^{1}H NMR (TMS, $CDCl_3$): δ 8.07 (m, 1H, CH), 7.82−7.6 (d and dt, 2H, CH), 7.11 (d, 1H, CH, *J* = 8.6 Hz), 7.00 (dt, 1H, CH, *J* = 6.7, 1.0 Hz), 4.90 (d, 1H, CH, *J* = 13.8 Hz), 3.15 (s, 3H, CH_3), 2.90 (s, 3H, CH_3). ^{11}B ($BF_3{\cdot}Et_2O$, $CDCl_3$): δ 0.114 (t). ^{13}C (TMS, $CDCl_3$): δ 168.7, 155.5, 154.3, 142.2, 137.7, 121.8, 116.5, 88.9, 45.2, 37.2. ^{15}N ($MeNO_2$, $CDCl_3$): δ −288.8, −181.8. ^{19}F ($CFCl_3$, $CDCl_3$): δ −141.8. Anal. Calcd for $C_{10}H_{12}BF_2N_3O$: C 50.25, H 5.06, N 17.58. Found: C 50.07, H 5.30, N 17.37.

*3-((1E,3E)-4-(Dimethylamino)buta-1,3-dien-1-yl)-1,1-difluoro-1H-pyrido[1,2-c][1,3,5,2]oxadiazaborinin-9-ium-1-uide (**B3**).* Yield of 0.40 g (54%). Mp 155.0−156.9 °C, dark orange powder. ^{1}H NMR (TMS, $CDCl_3$): δ 8.14 (bd, 1H, CH), 7.84 (dt, 1H, CH, *J* = 7.9, 1.8 Hz), 7.69 (dd, 1H, CH, *J* = 14.4, 11.9), 7.20 (d, 1H, CH, *J* = 8.6 Hz), 7.07 (dt, 1H, CH, *J* = 6.7, 1.0 Hz), 6.80 (d, 1H, CH, *J* = 13.0 Hz), 5.72 (d, 1H, CH, *J* = 14.4 Hz), 5.27 (dd, 1H, CH, *J* = 12.2 Hz), 2.95 (s, 6H, CH_3). ^{11}B ($BF_3{\cdot}Et_2O$, $CDCl_3$): δ 0.256 (t). ^{13}C (TMS, $CDCl_3$): δ 167.8, 155.4, 152.5, 149.8, 142.4, 137.9, 122.4, 117.5, 109.8, 98.1, 40.8. ^{15}N ($MeNO_2$, $CDCl_3$): δ −296.7, −178.2. ^{19}F ($CFCl_3$, $CDCl_3$): δ −140.7. Anal. Calcd for $C_{12}H_{14}BF_2N_3O$: C 54.37, H 5.32, N 15.85. Found: C 54.21, H 5.45, N 15.68.

*3-(4-(Dimethylamino)phenyl)-1,1-difluoro-1H-pyrido[1,2-c]-[1,3,5,2]oxadiazaborinin-9-ium-1-uide (**B4**).* Yield of 1.19 g (66%). Mp 167.0−168.7 °C, orange powder. ^{1}H NMR (TMS, $CDCl_3$): δ ∼8.26 (overlapped, 1H, CH), 8.24 (d, 2H, CH, *J* = 9.0 Hz), 7.97 (dt, 1H, CH, *J* = 7.9, 1.8 Hz), 7.43 (broadened d, 1H, CH, *J* = 8.2 Hz), 7.23 (dt, 1H, CH, *J* = 6.6, 1.1 Hz), 6.69 (d, 2H, CH, *J* = 9.0 Hz), 3.08 (s, 6H, CH_3). ^{11}B ($BF_3{\cdot}Et_2O$, $CDCl_3$): δ 0.495 (t). ^{13}C (TMS, $CDCl_3$): δ 166.1, 154.9, 153.9, 143.0, 138.2, 131.8, 122.9, 118.8, 118.5, 110.9, 40.1. ^{15}N ($MeNO_2$, $CDCl_3$): δ −318.3. ^{19}F ($CFCl_3$, $CDCl_3$): δ −139.6. Anal. Calcd for $C_{14}H_{14}BF_2N_3O$: C 58.17, H 4.88, N 14.54. Found: C 58.05, H 4.99, N 14.45.

*(E)-3-(4-(Dimethylamino)styryl)-1,1-difluoro-1H-pyrido[1,2-c]-[1,3,5,2]oxadiazaborinin-9-ium-1-uide (**B5**).* Yield of 0.64 g (45%). Mp 188.5−190.0 °C (dec), red powder. ^{1}H NMR (TMS, $CDCl_3$): δ 8.29 (d, 1H, CH, *J* = 5.8 Hz), 7.99 (dt, 1H, CH, *J* = 8.0 Hz, 1.8 Hz), 7.92 (d, 1H, CH, *J* = 15.6 Hz), 7.50 (d, 2H, CH, *J* = 8.8 Hz), 7.36 (d, 1H, CH, *J* = 8.44 Hz), 7.26 (dt, 1H, CH, *J* = 6.3, 1.2 Hz), 6.69 (d, 2H, *J* = 8.8 Hz), 6.52 (d, 1H, *J* = 15.6 Hz), 3.04 (s, 6H, CH_3). ^{11}B ($BF_3{\cdot}Et_2O$, $CDCl_3$): δ 0.356 (t). ^{13}C (TMS, $CDCl_3$): δ 170.0, 154.9, 152.0, 146.1, 143.3, 138.4, 130.4, 122.9, 122.5, 119.4, 115.4, 111.9, 40.1. ^{15}N ($MeNO_2$, $CDCl_3$): δ −321.6 (NMe_2), −175.8, −171.4. ^{19}F ($CFCl_3$, $CDCl_3$): δ −139.4. Anal. Calcd for $C_{16}H_{16}BF_2N_3O$: C 60.98, H 5.12, N 13.33. Found: C 60.84, H 5.27, N 13.09.

*3-((1E,3E)-4-(4-(Dimethylamino)phenyl)buta-1,3-dien-1-yl)-1,1-difluoro-1H-pyrido[1,2-c][1,3,5,2]oxadiazaborinin-9-ium-1-uide (**B6**).* Yield of 0.44 g (42%). Mp 228.0−230 °C (dec), red crystals. ^{1}H NMR (TMS, $CDCl_3$): δ 8.47 (d, 1H, CH, *J* = 5.4 Hz), 8.33 (dt, 1H, CH, *J* = 8.1, 1.7 Hz), 7.66 (dd, 1H, CH, *J* = 14.8, 10.9 Hz), 7.58 (dt, 1H, CH, *J* = 6.7, 1.2 Hz), 7.53 (d, 1H, CH, 8.4 Hz), 7.48 (d, 2H, CH, *J* = 8.9 Hz), 7.13 (d, 1H, CH, *J* = 15.0 Hz), 7.03 (dd, 1H, CH, *J* = 15.2, 10.9 Hz), 6.76 (d, 2H, CH, *J* = 8.9 Hz), 6.24 (d, 1H, CH, *J* = 15.0 Hz), 3.01 (s, 6H, CH_3). ^{11}B ($BF_3{\cdot}Et_2O$, DMSO-d_6): δ 0.241 (t). ^{13}C (TMS, DMSO-d_6): δ 165.4, 153.8, 151.5, 146.6, 145.7, 143.2, 139.2, 129.6, 124.0, 123.3, 122.4, 121.8, 121.4, 112.4, CH_3 overleaped by the solvent. ^{15}N ($MeNO_2$, DMSO-d_6): δ −322.2, −175.6, −166.9. ^{19}F ($CFCl_3$, $CDCl_3$): δ −137.0. Anal. Calcd for $C_{18}H_{18}BF_2N_3O$: C 63.37, H 5.32, N 12.32. Found: C 63.49, H 5.43, N 12.10.

*2,8-Bis(4-(dimethylamino)phenyl)-9a-fluoro-9aH-1,9-dioxa-3,3a^1,7-triaza-9a-boraphenalen-3a^1-ium-4-uide (**B7**).* Yield of 0.35 g (51%). Mp 284.4−286.2 °C, yellow-to-orange powder. ^{1}H NMR (TMS, $CDCl_3$): δ 8.24 (d, 4H, CH, *J* = 9.1 Hz), 7.86 (t, 1H, CH), 6.99 (d, 2H, CH, *J* = 8.1 Hz), 6.70 (d, 4H, CH, *J* = 9.1 Hz), 3.08 (s, 12H, CH_3). ^{11}B ($BF_3{\cdot}Et_2O$, DMSO-d_6): δ 1.098 (d). ^{13}C (TMS, DMSO-d_6): δ 165.5, 153.6, 150.6, 144.1, 131.5, 119.3, 110.9, 40.1. ^{15}N ($MeNO_2$, DMSO-d_6): δ −319.9, −175.6. ^{19}F ($CFCl_3$, $CDCl_3$): δ −126.1. Anal. Calcd for $C_{23}H_{23}BFN_5O_2$: C 64.05, H 5.38, N 16.24. Found: C 63.93, H 5.45, N 16.13.

■ ASSOCIATED CONTENT

Supporting Information

The Supporting Information is available free of charge on the ACS Publications website at DOI: 10.1021/acs.joc.5b02691.

NMR spectra, correlation charts, computational results, and Cartesian coordinates (PDF)

■ AUTHOR INFORMATION

Corresponding Authors

*E-mail: Denis.Jacquemin@univ-nantes.fr.

*E-mail: borys.osmialowski@utp.edu.pl

Notes

The authors declare no competing financial interest.

■ ACKNOWLEDGMENTS

A.M.G. acknowledges a statutory activity subsidy from the Polish Ministry of Science and Higher Education for the Faculty of Chemistry of Wrocław University of Technology. D.J. is a junior member of the Institut Universitaire de France. D.J. acknowledges the European Research Council (ERC) for financial support in the framework of a Starting Grant (Marches-278845). D.J. acknowledges the LUMOMAT project and his members for support. This research used resources of (i) the GENCI-CINES/IDRIS, (ii) the CCIPL (Centre de Calcul Intensif des Pays de Loire), and (iii) the Troy cluster in Nantes. Financial support from the National Science Centre (Grant No. 2013/09/B/ST5/03550) is gratefully acknowledged.

■ REFERENCES

(1) Kamkaew, A.; Lim, S. H.; Lee, H. B.; Kiew, L. V.; Chung, L. Y.; Burgess, K. *Chem. Soc. Rev.* **2013**, *42*, 77.

DOI: 10.1021/acs.joc.5b02691
J. Org. Chem. 2016, 81, 2280−2292

(2) Ulrich, G.; Ziessel, R.; Harriman, A. *Angew. Chem., Int. Ed.* **2008**, *47*, 1184.
(3) Zheng, Q.; Xu, G.; Prasad, P. N. *Chem. - Eur. J.* **2008**, *14*, 5812.
(4) Zhu, S.; Zhang, J.; Janjanam, J.; Vegesna, G.; Luo, F.-T.; Tiwari, A.; Liu, H. *J. Mater. Chem. B* **2013**, *1*, 1722.
(5) McCusker, C.; Carroll, J. B.; Rotello, V. M. *Chem. Commun.* **2005**, 996.
(6) Chen, T.; Boyer, J. H.; Trudell, M. L. *Heteroat. Chem.* **1997**, *8*, 51.
(7) Sathyamoorthi, G.; Wolford, L. T.; Haag, A. M.; Boyer, J. H. *Heteroat. Chem.* **1994**, *5*, 245.
(8) Ono, K.; Yamaguchi, H.; Taga, K.; Saito, K.; Nishida, J.-i.; Yamashita, Y. *Org. Lett.* **2009**, *11*, 149.
(9) Ono, K.; Hashizume, J.; Yamaguchi, H.; Tomura, M.; Nishida, J.-i.; Yamashita, Y. *Org. Lett.* **2009**, *11*, 4326.
(10) Fedorenko, E. V.; Mirochnik, A. G.; Beloliptsev, A. Y.; Isakov, V. V. *Dyes Pigm.* **2014**, *109*, 181.
(11) Gao, N.; Cheng, C.; Yu, C.; Hao, E.; Wang, S.; Wang, J.; Wei, Y.; Mu, X.; Jiao, L. *Dalton Trans.* **2014**, *43*, 7121.
(12) Yoshii, R.; Hirose, A.; Tanaka, K.; Chujo, Y. *J. Am. Chem. Soc.* **2014**, *136*, 18131.
(13) Wang, X.; Wu, Y.; Liu, Q.; Li, Z.; Yan, H.; Ji, C.; Duan, J.; Liu, Z. *Chem. Commun.* **2015**, *51*, 784.
(14) Kubota, Y.; Kasatani, K.; Takai, H.; Funabiki, K.; Matsui, M. *Dalton Trans.* **2015**, *44*, 3326.
(15) Ośmiałowski, B.; Zakrzewska, A.; Jędrzejewska, B.; Grabarz, A.; Zaleśny, R.; Bartkowiak, W.; Kolehmainen, E. *J. Org. Chem.* **2015**, *80*, 2072.
(16) Zakrzewska, A.; Zaleśny, R.; Kolehmainen, E.; Ośmiałowski, B.; Jędrzejewska, B.; Ågren, H.; Pietrzak, M. *Dyes Pigm.* **2013**, *99*, 957.
(17) Maar, R. R.; Barbon, S. M.; Sharma, N.; Groom, H.; Luyt, L. G.; Gilroy, J. B. *Chem. - Eur. J.* **2015**, *21*, 15589.
(18) Frath, D.; Azizi, S.; Ulrich, G.; Retailleau, P.; Ziessel, R. *Org. Lett.* **2011**, *13*, 3414.
(19) Telitel, S.; Blanchard, N.; Schweizer, S.; Morlet-Savary, F.; Graff, B.; Fouassier, J.-P.; Lalevée, J. *Polymer* **2013**, *54*, 2071.
(20) Frath, D.; Azizi, S.; Ulrich, G.; Ziessel, R. *Org. Lett.* **2012**, *14*, 4774.
(21) Uppal, T.; Hu, X.; Fronczek, F. R.; Maschek, S.; Bobadova-Parvanova, P.; Vicente, M. G. H. *Chem. - Eur. J.* **2012**, *18*, 3893.
(22) Ulrich, G.; Goze, C.; Guardigli, M.; Roda, A.; Ziessel, R. *Angew. Chem., Int. Ed.* **2005**, *44*, 3694.
(23) Papalia, T.; Siracusano, G.; Colao, I.; Barattucci, A.; Aversa, M. C.; Serroni, S.; Zappalà, G.; Campagna, S.; Sciortino, M. T.; Puntoriero, F.; Bonaccorsi, P. *Dyes Pigm.* **2014**, *110*, 67.
(24) Ziessel, R.; Ulrich, G.; Harriman, A.; Alamiry, M. A. H.; Stewart, B.; Retailleau, P. *Chem. - Eur. J.* **2009**, *15*, 1359.
(25) Bandi, V.; Das, S. K.; Awuah, S. G.; You, Y.; D'Souza, F. *J. Am. Chem. Soc.* **2014**, *136*, 7571.
(26) Galangau, O.; Dumas-Verdes, C.; Meallet-Renault, R.; Clavier, G. *Org. Biomol. Chem.* **2010**, *8*, 4546.
(27) Yu, C.; Jiao, L.; Yin, H.; Zhou, J.; Pang, W.; Wu, Y.; Wang, Z.; Yang, G.; Hao, E. *Eur. J. Org. Chem.* **2011**, *2011*, 5460.
(28) Hu, R.; Lager, E.; Aguilar-Aguilar, A.; Liu, J.; Lam, J. W. Y.; Sung, H. H. Y.; Williams, I. D.; Zhong, Y.; Wong, K. S.; Peña-Cabrera, E.; Tang, B. Z. *J. Phys. Chem. C* **2009**, *113*, 15845.
(29) Liu, J.-Y.; El-Khouly, M. E.; Fukuzumi, S.; Ng, D. K. P. *Chem. - Asian J.* **2011**, *6*, 174.
(30) Kostereli, Z.; Ozdemir, T.; Buyukcakir, O.; Akkaya, E. U. *Org. Lett.* **2012**, *14*, 3636.
(31) Di Donato, M.; Iagatti, A.; Lapini, A.; Foggi, P.; Cicchi, S.; Lascialfari, L.; Fedeli, S.; Caprasecca, S.; Mennucci, B. *J. Phys. Chem. C* **2014**, *118*, 23476.
(32) Huang, L.; Yu, X.; Wu, W.; Zhao, J. *Org. Lett.* **2012**, *14*, 2594.
(33) Rohand, T.; Baruah, M.; Qin, W.; Boens, N.; Dehaen, W. *Chem. Commun.* **2006**, 266.
(34) Jia, X.; Yu, X.; Zhang, G.; Liu, W.; Qin, W. *J. Coord. Chem.* **2013**, *66*, 662.
(35) Baruah, M.; Qin, W.; Vallée, R. A. L.; Beljonne, D.; Rohand, T.; Dehaen, W.; Boens, N. *Org. Lett.* **2005**, *7*, 4377.
(36) Yu, X.; Jia, X.; Yang, X.; Liu, W.; Qin, W. *RSC Adv.* **2014**, *4*, 23571.
(37) Du, M.-L.; Hu, C.-Y.; Wang, L.-F.; Li, C.; Han, Y.-Y.; Gan, X.; Chen, Y.; Mu, W.-H.; Huang, M. L.; Fu, W.-F. *Dalton Trans.* **2014**, *43*, 13924.
(38) Wu, Y.-Y.; Chen, Y.; Gou, G.-Z.; Mu, W.-H.; Lv, X.-J.; Du, M.-L.; Fu, W.-F. *Org. Lett.* **2012**, *14*, 5226.
(39) Wu, Y.-Y.; Chen, Y.; Mu, W.-H.; Lv, X.-J.; Fu, W.-F. *J. Photochem. Photobiol., A* **2013**, *272*, 73.
(40) Hand, E. S.; Baker, D. C. *Synthesis* **1989**, *1989*, 905.
(41) Massue, J.; Ulrich, G.; Ziessel, R. *Eur. J. Org. Chem.* **2013**, *2013*, 5701.
(42) Koyama, Y.; Matsumura, T.; Yui, T.; Ishitani, O.; Takata, T. *Org. Lett.* **2013**, *15*, 4686.
(43) Benelhadj, K.; Massue, J.; Retailleau, P.; Chibani, S.; Le Guennic, B.; Jacquemin, D.; Ziessel, R.; Ulrich, G. *Eur. J. Org. Chem.* **2014**, *2014*, 7156.
(44) Zhang, Z.; Zhang, H.; Jiao, C.; Ye, K.; Zhang, H.; Zhang, J.; Wang, Y. *Inorg. Chem.* **2015**, *54*, 2652.
(45) Gong, S.; Liu, Q.; Wang, X.; Xia, B.; Liu, Z.; He, W. *Dalton Trans.* **2015**, *44*, 14063.
(46) Riddle, J. A.; Lathrop, S. P.; Bollinger, J. C.; Lee, D. *J. Am. Chem. Soc.* **2006**, *128*, 10986.
(47) Macedo, F. P.; Gwengo, C.; Lindeman, S. V.; Smith, M. D.; Gardinier, J. R. *Eur. J. Inorg. Chem.* **2008**, *2008*, 3200.
(48) Yoshii, R.; Nagai, A.; Tanaka, K.; Chujo, Y. *Chem. - Eur. J.* **2013**, *19*, 4506.
(49) Benelhadj, K.; Massue, J.; Retailleau, P.; Ulrich, G.; Ziessel, R. *Org. Lett.* **2013**, *15*, 2918.
(50) Yoshii, R.; Tanaka, K.; Chujo, Y. *Macromolecules* **2014**, *47*, 2268.
(51) Kubota, Y.; Ozaki, Y.; Funabiki, K.; Matsui, M. *J. Org. Chem.* **2013**, *78*, 7058.
(52) Feng, J.; Liang, B.; Wang, D.; Xue, L.; Li, X. *Org. Lett.* **2008**, *10*, 4437.
(53) Frath, D.; Massue, J.; Ulrich, G.; Ziessel, R. *Angew. Chem., Int. Ed.* **2014**, *53*, 2290.
(54) Köhler, G.; Rechthaler, K.; Rotkiewicz, K.; Rettig, W. *Chem. Phys.* **1996**, *207*, 85.
(55) Dekhtyar, M.; Rettig, W.; Weigel, W. *Chem. Phys.* **2008**, *344*, 237.
(56) Grabowski, Z. R.; Rotkiewicz, K.; Rettig, W. *Chem. Rev.* **2003**, *103*, 3899.
(57) Murali, S.; Changenet-Barret, P.; Ley, C.; Plaza, P.; Rettig, W.; Martin, M. M.; Lapouyade, R. *Chem. Phys. Lett.* **2005**, *411*, 192.
(58) Ciofini, I.; Le Bahers, T.; Adamo, C.; Odobel, F.; Jacquemin, D. *J. Phys. Chem. C* **2012**, *116*, 11946.
(59) Lager, E.; Liu, J.; Aguilar-Aguilar, A.; Tang, B. Z.; Peña-Cabrera, E. *J. Org. Chem.* **2009**, *74*, 2053.
(60) Józefowicz, M.; Kozyra, K. A.; Heldt, J. R.; Heldt, J. *Chem. Phys.* **2005**, *320*, 45.
(61) Lakowicz, J. R. *Principles of Fluorescence Spectroscopy*; Springer: New York, 2006.
(62) Suppan, P. *J. Photochem. Photobiol., A* **1990**, *50*, 293.
(63) Koike, T.; Tanabe, M.; Takeuchi, N.; Tobinaga, S. *Chem. Pharm. Bull.* **1997**, *45*, 243.
(64) Iwano, S.; Obata, R.; Miura, C.; Kiyama, M.; Hama, K.; Nakamura, M.; Amano, Y.; Kojima, S.; Hirano, T.; Maki, S.; Niwa, H. *Tetrahedron* **2013**, *69*, 3847.
(65) Jouanin, I.; Sreevani, V.; Rathahao, E.; Guéraud, F.; Paris, A. *J. Labelled Compd. Radiopharm.* **2008**, *51*, 87.
(66) Kuhn, B.; Mohr, P.; Stahl, M. *J. Med. Chem.* **2010**, *53*, 2601.
(67) Glotzbach, C.; Kauscher, U.; Voskuhl, J.; Kehr, N. S.; Stuart, M. C. A.; Fröhlich, R.; Galla, H. J.; Ravoo, B. J.; Nagura, K.; Saito, S.; Yamaguchi, S.; Würthwein, E.-U. *J. Org. Chem.* **2013**, *78*, 4410.
(68) Brouwer, A. M. *Pure Appl. Chem.* **2011**, *83*, 2213.
(69) Chibani, S.; Laurent, A. D.; Le Guennic, B.; Jacquemin, D. *J. Chem. Theory Comput.* **2014**, *10*, 4574.
(70) Le Guennic, B.; Jacquemin, D. *Acc. Chem. Res.* **2015**, *48*, 530.

DOI: 10.1021/acs.joc.5b02691
J. Org. Chem. 2016, 81, 2280−2292

(71) Frisch, M. J.; Trucks, G. W.; Schlegel, H. B.; Scuseria, G. E.; Robb, M. A.; Cheeseman, J. R.; Scalmani, G.; Barone, V.; Mennucci, B.; Petersson, G. A.; Nakatsuji, H.; Caricato, M.; Li, X.; Hratchian, H. P.; Izmaylov, A. F.; Bloino, J.; Zheng, G.; Sonnenberg, J. L.; Hada, M.; Ehara, M.; Toyota, K.; Fukuda, R.; Hasegawa, J.; Ishida, M.; Nakajima, T.; Honda, Y.; Kitao, O.; Nakai, H.; Vreven, T.; Montgomery, J. A., Jr.; Peralta, J. E.; Ogliaro, F.; Bearpark, M. J.; Heyd, J.; Brothers, E. N.; Kudin, K. N.; Staroverov, V. N.; Kobayashi, R.; Normand, J.; Raghavachari, K.; Rendell, A. P.; Burant, J. C.; Iyengar, S. S.; Tomasi, J.; Cossi, M.; Rega, N.; Millam, N. J.; Klene, M.; Knox, J. E.; Cross, J. B.; Bakken, V.; Adamo, C.; Jaramillo, J.; Gomperts, R.; Stratmann, R. E.; Yazyev, O.; Austin, A. J.; Cammi, R.; Pomelli, C.; Ochterski, J. W.; Martin, R. L.; Morokuma, K.; Zakrzewski, V. G.; Voth, G. A.; Salvador, P.; Dannenberg, J. J.; Dapprich, S.; Daniels, A. D.; Farkas, Ö.; Foresman, J. B.; Ortiz, J. V.; Cioslowski, J.; Fox, D. J. *Gaussian 09*, revision D01; Gaussian, Inc.: Wallingford, CT, USA, 2009.

(72) Shao, Y.; Gan, Z.; Epifanovsky, E.; Gilbert, A. T. B.; Wormit, M.; Kussmann, J.; Lange, A. W.; Behn, A.; Deng, J.; Feng, X.; Ghosh, D.; Goldey, M.; Horn, P. R.; Jacobson, L. D.; Kaliman, I.; Khaliullin, R. Z.; Kuś, T.; Landau, A.; Liu, J.; Proynov, E. I.; Rhee, Y. M.; Richard, R. M.; Rohrdanz, M. A.; Steele, R. P.; Sundstrom, E. J.; Woodcock, H. L.; Zimmerman, P. M.; Zuev, D.; Albrecht, B.; Alguire, E.; Austin, B.; Beran, G. J. O.; Bernard, Y. A.; Berquist, E.; Brandhorst, K.; Bravaya, K. B.; Brown, S. T.; Casanova, D.; Chang, C.-M.; Chen, Y.; Chien, S. H.; Closser, K. D.; Crittenden, D. L.; Diedenhofen, M.; DiStasio, R. A.; Do, H.; Dutoi, A. D.; Edgar, R. G.; Fatehi, S.; Fusti-Molnar, L.; Ghysels, A.; Golubeva-Zadorozhnaya, A.; Gomes, J.; Hanson-Heine, M. W. D.; Harbach, P. H. P.; Hauser, A. W.; Hohenstein, E. G.; Holden, Z. C.; Jagau, T.-C.; Ji, H.; Kaduk, B.; Khistyaev, K.; Kim, J.; Kim, J.; King, R. A.; Klunzinger, P.; Kosenkov, D.; Kowalczyk, T.; Krauter, C. M.; Lao, K. U.; Laurent, A. D.; Lawler, K. V.; Levchenko, S. V.; Lin, C. Y.; Liu, F.; Livshits, E.; Lochan, R. C.; Luenser, A.; Manohar, P.; Manzer, S. F.; Mao, S.-P.; Mardirossian, N.; Marenich, A. V.; Maurer, S. A.; Mayhall, N. J.; Neuscamman, E.; Oana, C. M.; Olivares-Amaya, R.; O'Neill, D. P.; Parkhill, J. A.; Perrine, T. M.; Peverati, R.; Prociuk, A.; Rehn, D. R.; Rosta, E.; Russ, N. J.; Sharada, S. M.; Sharma, S.; Small, D. W.; Sodt, A. *Mol. Phys.* **2015**, *113*, 184.

(73) Chibani, S.; Le Guennic, B.; Charaf-Eddin, A.; Maury, O.; Andraud, C.; Jacquemin, D. *J. Chem. Theory Comput.* **2012**, *8*, 3303.

(74) Zhao, Y.; Truhlar, D. *Theor. Chem. Acc.* **2008**, *120*, 215.

(75) Yanai, T.; Tew, D. P.; Handy, N. C. *Chem. Phys. Lett.* **2004**, *393*, 51.

(76) Adamo, C.; Barone, V. *J. Chem. Phys.* **1999**, *110*, 6158.

(77) Tomasi, J.; Mennucci, B.; Cammi, R. *Chem. Rev.* **2005**, *105*, 2999.

(78) Caricato, M.; Mennucci, B.; Tomasi, J.; Ingrosso, F.; Cammi, R.; Corni, S.; Scalmani, G. *J. Chem. Phys.* **2006**, *124*, 124520.

(79) Ferrer, F. J. A.; Improta, R.; Santoro, F.; Barone, V. *Phys. Chem. Chem. Phys.* **2011**, *13*, 17007.

(80) Le Bahers, T.; Adamo, C.; Ciofini, I. *J. Chem. Theory Comput.* **2011**, *7*, 2498.

(81) Jacquemin, D.; Bahers, T. L.; Adamo, C.; Ciofini, I. *Phys. Chem. Chem. Phys.* **2012**, *14*, 5383.

(82) Andrews, D. L.; Rodríguez, J. *J. Chem. Phys.* **2007**, *127*, 084509.

(83) Santoro, F.; Lami, A.; Improta, R.; Barone, V. *J. Chem. Phys.* **2007**, *126*, 184102.

(84) Santoro, F.; Barone, V.; Improta, R. *J. Comput. Chem.* **2008**, *29*, 957.

(85) Avila Ferrer, F. J.; Cerezo, J.; Stendardo, E.; Improta, R.; Santoro, F. *J. Chem. Theory Comput.* **2013**, *9*, 2072.

DOI: 10.1021/acs.joc.5b02691
J. Org. Chem. 2016, 81, 2280−2292